

## Supporting Information

### Balancing Effect between Adsorption and Diffusion on Catalytic Performance Inside Hollow Nanostructured Catalyst

Dawei Yao,<sup>†</sup> Yue Wang<sup>\*†</sup>, Katherine Hassan-Legault,<sup>‡</sup> Antai Li<sup>†</sup>, Yujun Zhao<sup>†</sup>, Jing Lv<sup>†</sup>, Shouying Huang<sup>†</sup> and Xinbin Ma<sup>\*†</sup>

<sup>†</sup>Key Laboratory for Green Chemical Technology of Ministry of Education, Collaborative Innovation Center of Chemical Science and Engineering, School of Chemical Engineering and Technology, Tianjin University, Tianjin 300072, People's Republic of China

<sup>‡</sup> Department of Chemical and Biological Engineering, University of Ottawa, Ontario K1N 6N5, Canada

## **1 Experimental section**

### **Catalyst preparation**

Synthesis of the silica spheres was performed using a Stöber method described in literature.<sup>1</sup> To fabricate 211 nm silica spheres, 9 mL ammonia solution (25%; J&K Co.) was added to 25 mL deionized water, followed by the addition of a mixture of 8 mL tetraethyl orthosilicate (TEOS, 98%; Sigma-Aldrich) and 45.5 mL dehydrated ethanol (99.8%; J&K Co.). To obtain the silica sphere suspension, the mixture of TEOS, ethanol, ammonia and water was stirred at 313 K for 2 h. The other sizes of silica spheres were obtained by changing the ratio of ethanol, water and ammonia. The silica spheres were separated from suspension and washed with ethanol and deionized water, then dispersed into 60 mL deionized water again for the following fabrication process.

Copper silicate NAHSs were fabricated by a modified method. To fabricate a NAHS with 211 nm hollow sphere size and 70 nm nanotube length, 6.09 g of copper nitrate (99%; Sigma-Aldrich) and 19 mL ammonia solution were added into 200 mL deionized water, followed by drop-wise addition of the 60 mL silica sphere suspension. This mixture was transferred into an autoclave, heated at 413 K for 5 h to generate the 70 nm nanotubes. Then, the sample was washed by deionized water several times until the rest of copper ions were removed. The separated powder was mixed with ammonia solution (1.25%) and transferred into the autoclave again for the hydrothermal treatment to dissolve the rest of silica core. The obtained mixture was separated and washed with distilled water until the pH value reached 7.0, then dried under vacuum at 355 K for

6 h. These as-synthesized samples were calcined in static air at 723 K for 4 h, tableted, crushed, and sieved to 40-60 meshes.

### **Catalytic activity test**

The catalytic performance was tested in a fixed-bed reaction system. 0.4g of catalyst (40-60 meshes) was placed in the certain zone of the reaction tube where the temperature could be maintained constant. Before the reaction, the catalyst was first reduced by hydrogen at 573 K for 4 h and then decreased to reaction temperature. The feed (20 wt. % DMO, dissolved in methanol) was injected into the fixed-bed reaction system continuously with a certain weight hourly space velocity (WHSV). To obtain the reaction rate, the evaluation was taken under severe conditions, where the DMO conversion kept below 70%. The reaction products were condensed, collected, then analyzed on the Agilent Micro GC 6820, which is equipped with a HP-INNOWAX capillary column (Hewlett-Packard Company, 30 m×0.32 mm×0.50 μm), as well as a flame ionization detector (FID).

The apparent reaction rate,  $R_{\text{site}}$  values (the conversion rate of DMO normalized by the amount of surface  $\text{Cu}^0$  or  $\text{Cu}^+$  sites) were calculated from equation S1-1 to S1-3

$$\text{Apparent reaction rate} = \frac{\text{Total DMO converted } (\text{mol}\cdot\text{h}^{-1}\cdot\text{g}_{\text{cat}}^{-1})}{\text{Total amount of surface copper } (\text{mol}\cdot\text{g}_{\text{cat}}^{-1})} \quad (\text{S1-1})$$

$$R_{\text{site-Cu(0)}} = \frac{\text{Total DMO converted } (\text{mol}\cdot\text{h}^{-1}\cdot\text{g}_{\text{cat}}^{-1})}{\text{Total amount of surface Cu(0) } (\text{mol}\cdot\text{g}_{\text{cat}}^{-1})} \quad (\text{S1-2})$$

$$R_{\text{site-Cu(I)}} = \frac{\text{Total DMO converted } (\text{mol}\cdot\text{h}^{-1}\cdot\text{g}_{\text{cat}}^{-1})}{\text{Total amount of surface Cu(I) } (\text{mol}\cdot\text{g}_{\text{cat}}^{-1})} \quad (\text{S1-3})$$

## Characterization

Pore structure of the samples was determined at 77 K by a N<sub>2</sub> adsorption-desorption method using a Micromeritics Tristar II 3000 Analyzer. Barrett-Joyner-Halenda (BJH) method is used to calculate the pore-size distribution. Brunauer-Emmett-Teller (BET) method is applied to calculate the specific surface area.

The copper content of samples was analyzed by using Inductively Coupled Plasma Optical Emission Spectrometer (ICP-OES, Varian Vista-MPX), and was determined by the Cu characteristic peak at 324.754 nm.

Transmission electron microscopy (TEM) images were obtained by a Philips TECNAI G2 F20 system electron microscope. The samples were dispersed in ethanol, dropped onto a copper grid-supported carbon membrane and dried. For each sample, 200 nanotubes were measured to obtain the length distribution of nanotubes, 100 hollow spheres were measured to determine the hollow-sphere size, and 200 copper nanoparticles were counted to calculate the average particle size at least.

The N<sub>2</sub>O titration is used to determine the metallic copper surface area by using a Micromeritics Autochem II 2920 apparatus. Briefly, a 50 mg sample was first reduced in hydrogen for 2 h at 573 K, then treated by N<sub>2</sub>O flow at 363 K to completely oxidized the surface metallic copper to Cu<sub>2</sub>O. Finally, the sample was reduced again at 573 K by pulse titration using 10% H<sub>2</sub>/Ar. By assuming spherical shape of copper particles and  $1.47 \times 10^{19}$  copper atoms/m<sup>2</sup>, the copper surface area ( $S_{Cu(0)}$ ) could be calculated by following equation:

$$S_{Cu(0)} = \frac{2 \times C_H \times N_A}{w_{cat} \times 1.47 \times 10^{19}} (m^2 g_{cat}^{-1}) \quad (S1-4)$$

where  $C_H$ : Hydrogen consumption in pulse chemisorption step (mol);

$N_A$ : Avogadro's constant;

$w_{cat}$ : weigh of catalyst (g).

X-ray diffraction (XRD) was conducted by a Rigaku C/max-2500 diffractometer, employing the graphite-filtered Cu K $\alpha$  radiation ( $\lambda=1.5406 \text{ \AA}$ ) at room temperature. The reduced samples were scanned from  $10^\circ$  to  $90^\circ$  with a rate of  $8^\circ/\text{min}$ .

Fourier-transform Infrared (FTIR) spectra of samples was recorded from  $500 \text{ cm}^{-1}$  to  $1900 \text{ cm}^{-1}$  by a Nicolet 6700 spectrometer equipped with a DTGS detector. The sample was mixed with KBr and pelletized before scanning. The spectral resolution was  $4 \text{ cm}^{-1}$ , and 32 scans were conducted for each spectrum recording.

The in situ FTIR of CO adsorption was performed by the Nicolet 6700 spectrometer equipped with a MCT/A detector and a vacuum system. Briefly, the calcined sample (16-17 mg) was tableted and placed into the in situ cell. Then the sample was reduced under hydrogen flow at 573 K for 1 h, then exposed to the flow of CO at 303 K for 30 min. The evacuation was performed to remove CO molecules in the gas phase and the ones that were weakly adsorbed on the sample, until the scanned spectra no longer changed.

X-ray photoelectron spectra (XPS) and Auger electron spectroscopy (AES) were conducted by a Kratos XSAM 800 spectrometer with Al K $\alpha$  X-ray radiation source ( $h\nu = 1486.6 \text{ eV}$ ). Before the measurement, the sample was tableted and reduced in  $H_2$  at 573 K for 4 h. The obtained binding

energy was calibrated using the Si 2p peak at 103.2 eV as the reference. The experimental error was within  $\pm 0.2$  eV.

The high-pressure hydrogen adsorption was carried out on a pressure composition isothermal system (Micromeritics ASAP 2050). The sample was reduced at 573 K in a flow of hydrogen before measurement. A stainless steel tube was loaded with 2 g of the reduced sample and subsequently connected to the manometric instrument. Pretreatment was conducted under vacuum at 573 K for 2 h to remove water and other adsorbed molecules. Then, the hydrogen was injected into the sample tube at 463 K to increase the pressure gradually to 10 MPa. The pressure-composition-isotherms were recorded at the same time. The pressure was measured by a capacitance manometer with an error of 1%.

### **Computational Method**

All DFT calculations were performed using the Dmol<sup>3</sup> program package of Materials Studio. The geometry optimizations as well as energy calculations were performed using a double numerical basis set with polarization (DNP)<sup>2</sup>. The generalized gradient approximation (GGA) with Perdew–Burke–Ernzerh (PBE)<sup>3</sup> was used for describing electron exchange and correlation effects. The convergence tolerance of total energy, force, and displacement were less than  $2 \times 10^{-5}$  Ha,  $4 \times 10^{-3}$  Ha/Å and  $5 \times 10^{-3}$  Å, respectively. All atoms were treated with all electron basis sets.

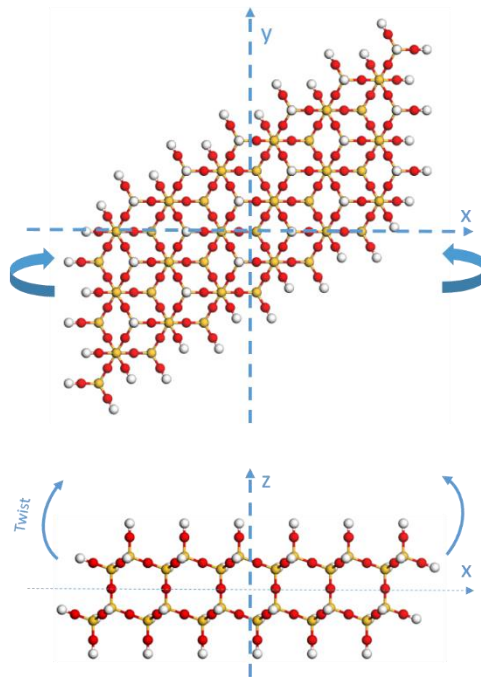
The crystal structure of SiO<sub>2</sub> (111) planar surface was modeled by a eleven-layer slab, with the bottom five layers fixed. The edge of the cluster was terminated by adding H atoms to form O–H groups to maintain charge neutrality. The curved SiO<sub>2</sub> surfaces with different curvature were

modeled by twist SiO<sub>2</sub> (111) planar surface around y axis (Scheme S1). For calculations regarding H<sub>2</sub> adsorption on SiO<sub>2</sub> surface, the adsorbed H<sub>2</sub> are sitting above the –OH group on the curved silica surface, with a distance of around 3 Å. The structures of all optimized structures are shown in Figure 6.

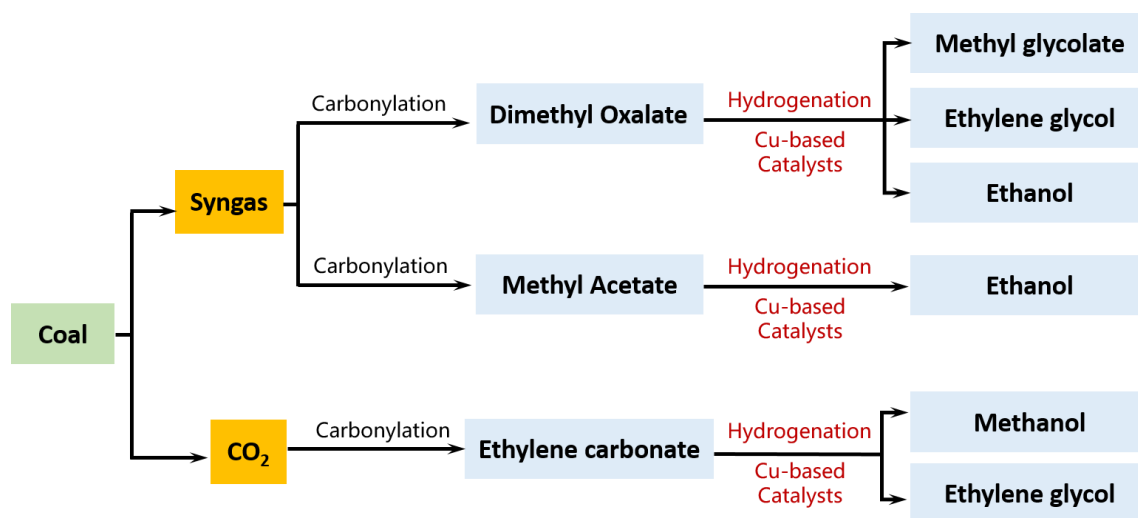
In order to explain the interaction intensity between the H<sub>2</sub> and SiO<sub>2</sub> surface, the adsorption energy of H<sub>2</sub> were calculated by equation (S1-5):

$$E_{\text{ads}} = E_{\text{surface}} + E_{\text{H}_2} - E_{\text{surface-H}_2} \quad (\text{S1-5})$$

where  $E_{\text{ads}}$  is the adsorption energy,  $E_{\text{surface}}$  is the total energy of SiO<sub>2</sub> surface,  $E_{\text{H}_2}$  is the energy of H<sub>2</sub> molecule,  $E_{\text{surface-H}_2}$  is the total energy of SiO<sub>2</sub> surface and H<sub>2</sub> after adsorption.



**Scheme S1.** SiO<sub>2</sub>(111) surface with coordinate.



**Scheme S2.** Route of coal to oxygenated compounds.

## 2 Hydrothermal method for NAHS fabrication

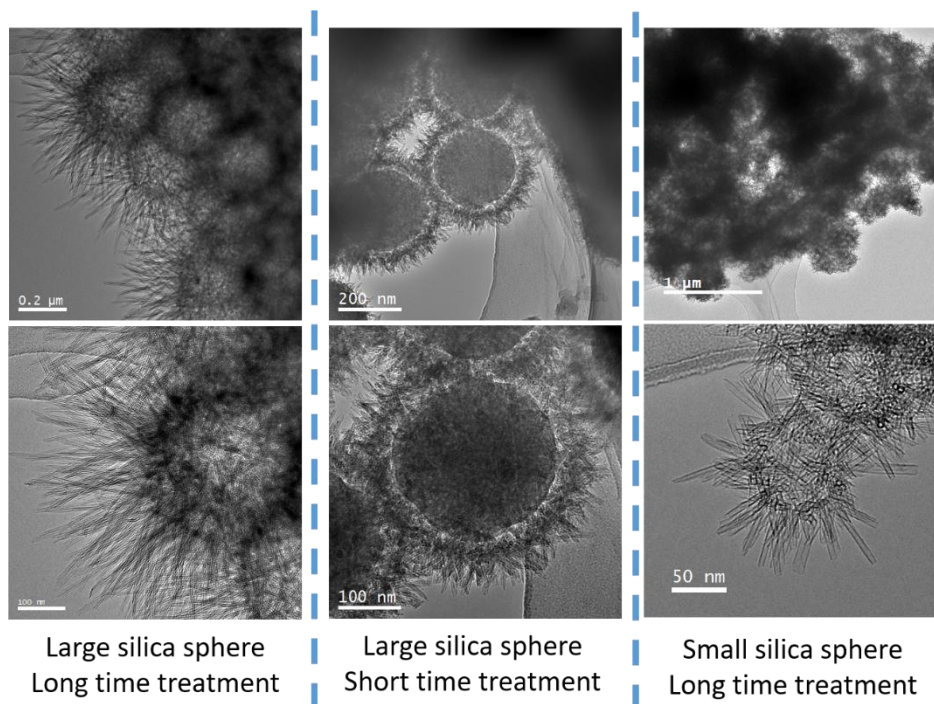
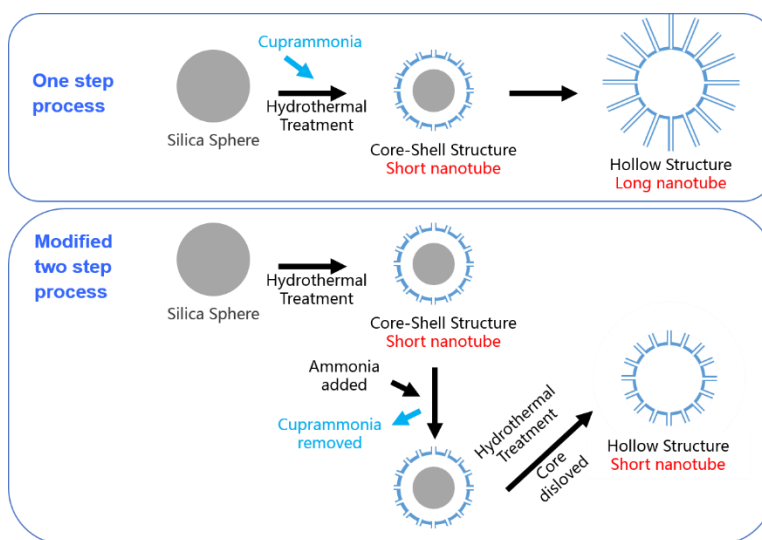


**Figure S1.** TEM images in one step process for NAHS fabrication.



**Scheme S3.** Comparison of two processes for fabricating the NAHSs.

### 3 Physical properties on NAHSs

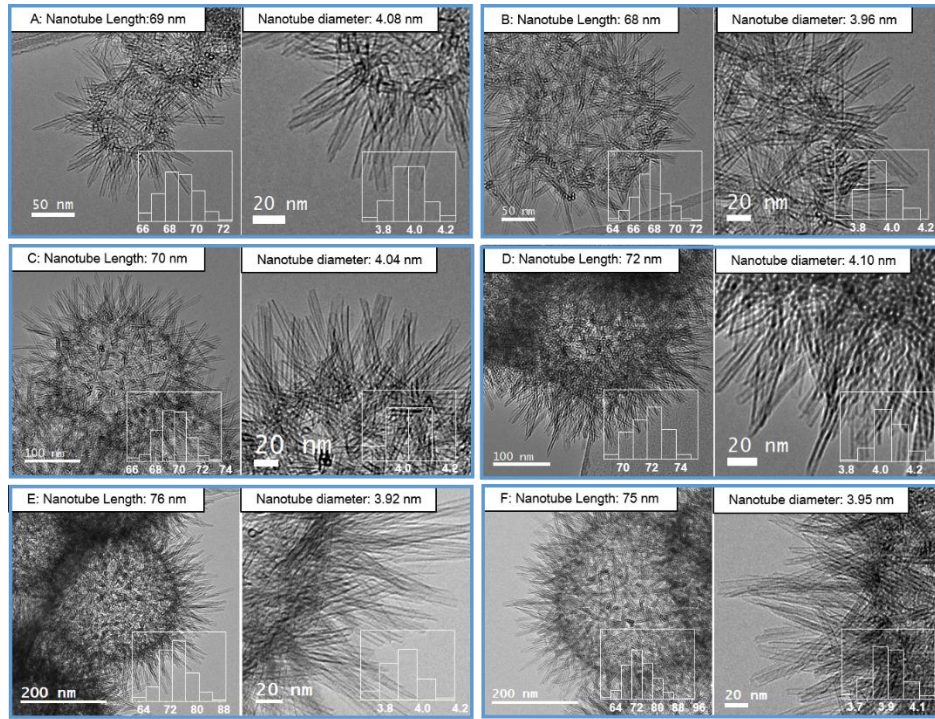


**Figure S2.** TEM images of calcined NAHSs. Hollow sphere size: 69 nm(A), 140 nm(B), 211 nm(C), 258 nm(D), 325 nm(E) and 361 nm(F).

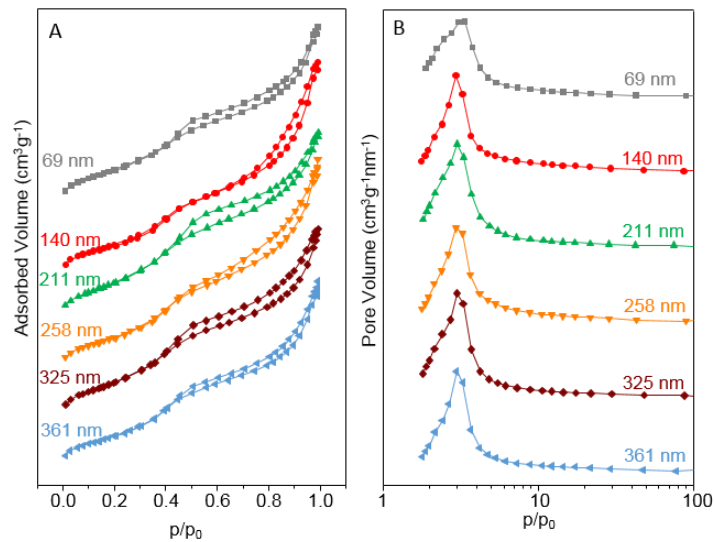


**Figure S3.**  $N_2$  adsorption-desorption isotherms (A) and pore size distributions (B) of all the NAHSs with different hollow-sphere sizes.

**Table S1.** Physical properties of NAHS, NTs and lamellar-structured Cu/SiO<sub>2</sub>.

Hollow-sphere Diameter (nm) <sup>a</sup>	Length of nanotubes (nm) <sup>a</sup>	Diameter of nanotubes (nm) <sup>a</sup>	Pore volume (cm <sup>3</sup> /g) <sup>b</sup>	Pore Size (nm) <sup>b</sup>	Specific surface area (m <sup>2</sup> /g) <sup>b</sup>
69±5	69	4.08	0.67	5.16	407
140±9	68	3.96	0.68	5.25	399
211±10	70	4.04	0.69	4.64	455
258±6	72	4.10	0.67	5.69	401
325±8	76	3.92	0.70	4.81	412
361±9	75	3.95	0.68	5.41	385

[a] Average size that measured from more than 100-200 hollow spheres or nanotubes in TEM images;

[b] Determined by N<sub>2</sub> adsorption-desorption method.

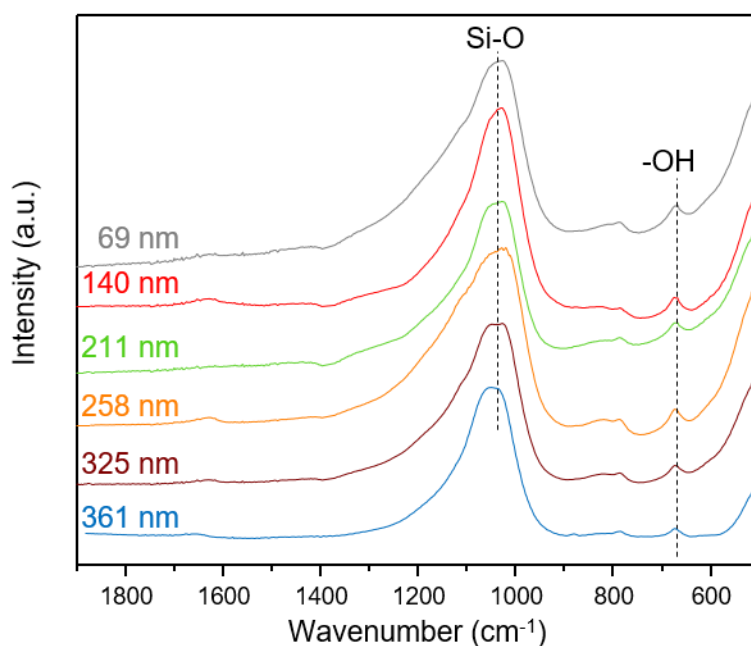


**Figure S4.** FTIR spectra of calcined NAHSs with different hollow-sphere sizes.

#### 4 Active species of NAHSs

**Table S2.** Characterization of Cu species on catalysts.

Hollow sphere size (nm)	Cu loading <sup>a</sup> (%)	Particle size <sup>b</sup> (nm)	S <sub>Cu(0)</sub> <sup>c</sup> (m <sup>2</sup> /g)	S <sub>Cu(I)</sub> <sup>d</sup> (m <sup>2</sup> /g)	A <sub>Cu(I)</sub> <sup>e</sup> (area/g)	Cu <sup>+</sup> /(Cu <sup>0</sup> +Cu <sup>+</sup> ) <sup>f</sup> (%)
69	33.9	3.5	33.6	8.9	207	21.1
140	32.0	3.7	30.4	9.3	212	23.5
211	32.0	3.7	30.3	9.1	232	23.1
258	32.8	3.6	31.8	9.0	207	22.2
325	31.5	3.5	33.4	10.1	238	23.2
361	30.6	3.4	33.5	9.7	225	22.5

<sup>a</sup>Determined by ICP-OES <sup>b</sup>Calculated from XRD patterns by using the Scherrer equation. <sup>c</sup> Determined by N<sub>2</sub>O titration. <sup>d</sup>Calculated on the basis of S<sub>Cu(0)</sub> and X<sub>Cu(I)</sub> and verified by in situ FTIR spectra of CO adsorption. <sup>e</sup>Integral area under the peaks in the FTIR spectra of CO adsorption on active Cu(I) on the surface of catalysts after evacuation <sup>f</sup>Calculated from Cu LMM AES spectra.

## 5 Effect of Hollow-Sphere Size on Catalytic performance

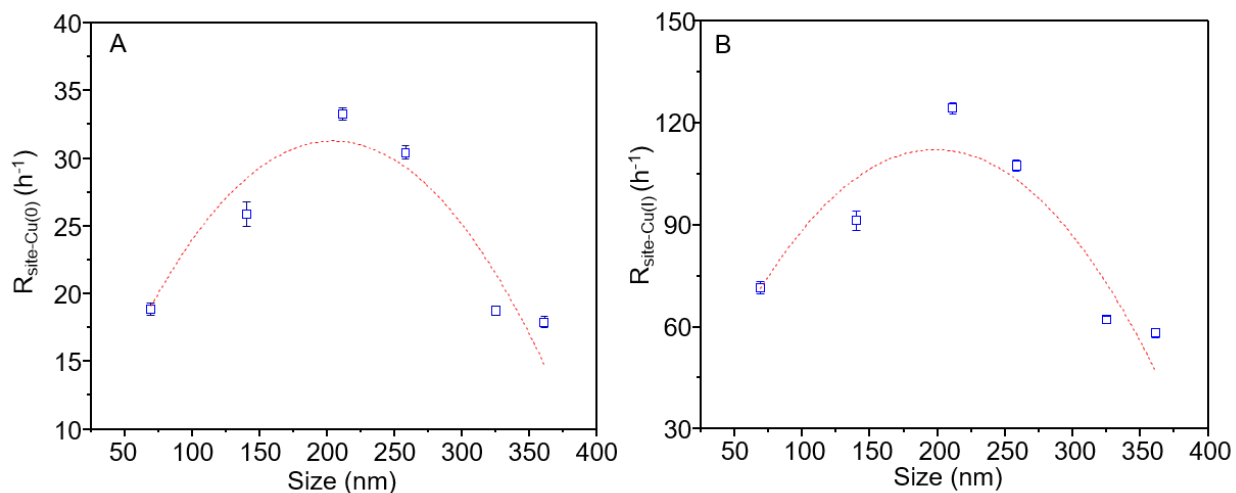


**Figure S5.**  $R_{\text{site-Cu(0)}}$  (A) and  $R_{\text{site-Cu(I)}}$  (B) of NAHSs with different hollow-sphere size for DMO hydrogenation. The  $R_{\text{site-Cu(0)}}$  and  $R_{\text{site-Cu(I)}}$  are calculated from the conversion rate normalized by the amounts of surface  $\text{Cu}^0$  or  $\text{Cu}^+$  sites. Reaction condition: 463 K, 2.5 MPa,  $\text{H}_2/\text{DMO} = 20$ .

## 6 Effect of Hollow-Sphere Size on Hydrogen Enrichment

**Table S3.** H<sub>2</sub> chemisorption capacity on NAHSs with different hollow-sphere size

Hollow-sphere Size (nm)	H <sub>2</sub> Chemisorption ( $\mu\text{mol/g}$ ) <sup>a</sup>
69	173.1
140	169.2
211	162.0
258	168.5
325	162.4
361	168.6

<sup>a</sup> Determined by H<sub>2</sub>-TPD.

## 7 Determination of mass transfer effect on catalytic performance

Kinetic parameters of chemical reactions are extensively studied to estimate the external and internal mass-transfer effects. The external diffusion can be estimated by calculating the Carberry number ( $C_a$ )<sup>4-6</sup>: when this number is less than 0.05, the reaction is not limited by external mass transfer between solid catalyst and gaseous reactant.<sup>4, 7</sup>  $C_a$  can be calculated by observed reaction rate and the maximum mass-transfer rate,

$$C_a = \frac{r_{obs}}{k_g a_s (C_i^* - C_i^0)} \quad (S7-1)$$

where  $r_{obs}$  ( $\text{mol s}^{-1} \text{g}_{\text{cat}}^{-1}$ ) is observed reaction rate;  $a_s$  ( $\text{m}^2 \text{g}^{-1}$ ) is the external catalyst specific surface area;  $C_i^*$  ( $\text{mol m}^{-3}$ ) is the concentration of the reactant in bulk phase; and  $k_g$  ( $\text{m g}^{-3} \text{ms}^{-2} \text{s}^{-1}$ ) is the solid-gas mass transfer coefficient, which can be calculated by equation (S7-2),<sup>8-9</sup>

$$k_g = \frac{D_B}{R} Sc^{1/3} Re J_D \quad (S7-2)$$

where  $Sc$  and  $Re$  are the Schmidt and Reynolds number respectively;  $D_B$  is the bulk diffusion coefficient for a multicomponent mixture, which can be calculated by equations (S7-3) and (S7-4)<sup>10</sup>:

$$\frac{1}{D_B} = \frac{1}{1-y_i} \sum_j^n \frac{y_j}{D_{ij}} \quad (S7-3)$$

where  $D_{ij}$  is the diffusion coefficients for a binary mixture of  $i$  and  $j$ , which can be calculated by reaction temperature, pressure, molar mass and summing atomic diffusion volumes<sup>10</sup>:

$$D_{ij} = \frac{1 \times 10^{-3} T^{\frac{3}{2}}}{P \left[ (\sum V)_i^{\frac{1}{3}} + (\sum V)_j^{\frac{1}{3}} \right]^2} \left[ \frac{1}{M_i} + \frac{1}{M_j} \right]^{\frac{1}{2}} \quad (S7-4)$$

Meanwhile,  $J_D$  is the Colburn J factor<sup>8-9</sup>. When  $Re$  is higher than 10 in fixed bed system,  $J_D$  can be calculated by equation (S7-5)<sup>11</sup>:

$$J_D = \frac{0.765}{Re^{0.82}} + \frac{0.365}{Re^{0.386}} \quad (S7-5)$$

Furthermore, the Wheeler-Weisz criterion ( $\eta\phi^2$ ) is applied to determine the influence of inner mass transfer diffusion. When the Wheeler-Weisz criterion is higher than 0.1, the effect of mass transfer of the reactant on the reaction can't be neglected.<sup>12-13</sup> The Wheeler-Weisz criterion is defined in equation (S7-6):

$$\eta\phi^2 = \frac{r_{obs}R^2}{D_{eff}C_i^*} \quad (S7-6)$$

where  $r_{obs}$  ( $\text{mol s}^{-1} \text{g}_{\text{cat}}^{-1}$ ) is the observed reaction rate;  $R$  (m) is the radius of the catalyst particle;  $C_i^*$  ( $\text{mol} \cdot \text{m}^{-3}$ ) is the surface concentration of the reactant;  $D_{eff}$  ( $\text{m}^2 \cdot \text{s}^{-1}$ ) is the effective diffusion coefficient in the pores of the catalysts. The effective diffusion coefficient is given by equation (S7-7):

$$D_{eff} = \frac{\varepsilon}{\tau} D_p \quad (S7-7)$$

where  $\varepsilon$  is the porosity of the catalysts and  $\tau$  is the tortuosity factor.

The calculated Carberry number and Wheeler-Weisz criterions of DMO in all the NAHSs are listed in Table S4. Evidently, the Carberry numbers of NAHSs with different hollow-sphere sizes are from  $5.8 \times 10^{-6}$  to  $17.3 \times 10^{-6}$ , which are much lower than the value of 0.05. This demonstrates that the reaction is not influenced by external diffusion. In comparison, all the Wheeler-Weisz criterions listed in Table S4 are higher than the value of 0.1, which indicates the existence of diffusion limitation.

**Table S4.** Calculated Carberry number and Wheeler-Weisz Group.

	Size of hollow sphere (nm)	Conversion (%)	$r_{\text{obs}}$ ( $10^{-6}$ mol/s/g <sub>cat</sub> )	Carberry number	Wheeler-Weisz group
MA Hydrogenation	69	84.3	$0.33 \times 10^{-6}$	$0.87 \times 10^{-6}$	$4.7 \times 10^{-3}$
	140	73.4	$0.40 \times 10^{-6}$	$1.32 \times 10^{-6}$	$4.1 \times 10^{-3}$
	211	69.1	$0.48 \times 10^{-6}$	$1.77 \times 10^{-6}$	$3.9 \times 10^{-3}$
	258	68.5	$0.47 \times 10^{-6}$	$1.94 \times 10^{-6}$	$3.8 \times 10^{-3}$
	325	64.4	$0.32 \times 10^{-6}$	$0.81 \times 10^{-6}$	$3.6 \times 10^{-3}$
	361	64.5	$0.27 \times 10^{-6}$	$0.65 \times 10^{-6}$	$3.6 \times 10^{-3}$
DMO Hydrogenation	69	42.6	$9.79 \times 10^{-6}$	$7.8 \times 10^{-6}$	0.15
	140	52.3	$12.0 \times 10^{-6}$	$11.8 \times 10^{-6}$	0.16
	211	69.5	$14.2 \times 10^{-6}$	$15.7 \times 10^{-6}$	0.20
	258	65.0	$14.1 \times 10^{-6}$	$17.3 \times 10^{-6}$	0.22
	325	42.0	$9.47 \times 10^{-6}$	$7.2 \times 10^{-6}$	0.15
	361	38.1	$7.98 \times 10^{-6}$	$5.8 \times 10^{-6}$	0.12
DEO Hydrogenation	69	43.8	$12.2 \times 10^{-6}$	$15.6 \times 10^{-6}$	0.14
	140	53.7	$15.0 \times 10^{-6}$	$23.6 \times 10^{-6}$	0.17
	211	63.9	$17.8 \times 10^{-6}$	$31.6 \times 10^{-6}$	0.20
	258	63.2	$17.6 \times 10^{-6}$	$34.8 \times 10^{-6}$	0.20
	325	42.4	$11.8 \times 10^{-6}$	$14.5 \times 10^{-6}$	0.13
	361	35.7	$9.98 \times 10^{-6}$	$11.7 \times 10^{-6}$	0.11

Reaction Conditions: 463 K, 2.5 MPa, H<sub>2</sub>/Ester=20, WHSV<sub>MA</sub>=0.2 h<sup>-1</sup>, WHSV<sub>DMO</sub>=6.4 h<sup>-1</sup>, WHSV<sub>DEO</sub>=11.9 h<sup>-1</sup>

The Carberry number<sup>4-6</sup> and Wheeler-Weisz criterion<sup>12-13</sup> are calculated to verify the influence of external and internal mass transfer limitation. If the Carberry number is smaller than 0.05, the reaction is not limited by the external mass transfer. Meanwhile, if the Wheeler-Weisz criterions is smaller than 0.1, the reaction is not limited by internal mass transfer. Table S4 indicates that the external diffusion is not limited in all the hydrogenation reactions. The internal diffusion limitation is not present in MA hydrogenation, while the DEO and DMO hydrogenations are limited by internal diffusion.

## 8 Calculation of diffusion coefficient

The ratio of the mean free path of DMO and pore diameter of NAHSs is 7.81, which is between 0.01 and 10. Therefore, in the calculation of diffusion coefficient, the bulk diffusion (caused by the collision between molecules) and Knudsen diffusion (caused by the collision between the molecule and pore wall). Meanwhile, the diffusion coefficient ( $D_p$ ,  $m^2 \cdot s^{-1}$ ) can be calculated by Bosanquet formula:<sup>10</sup>

$$\frac{1}{D_p} = \frac{1}{D_K} + \frac{1}{D_B} \quad (\text{S8-1})$$

The  $D_B$  is the bulk diffusion coefficient for a multicomponent mixture, which can be calculated by equations (S8-2) and (S8-3)<sup>10</sup>:

$$\frac{1}{D_B} = \frac{1}{1-y_i} \sum_j^n \frac{y_j}{D_{ij}} \quad (\text{S8-2})$$

where  $D_{ij}$  is the diffusion coefficients for a binary mixture of i and j, which can be calculated by reaction temperature, pressure, molar mass and summing atomic diffusion volumes<sup>10</sup>:

$$D_{ij} = \frac{1 \times 10^{-3} T^{\frac{3}{2}}}{P [(\sum V)_i^{\frac{1}{3}} + (\sum V)_j^{\frac{1}{3}}]^2} \left[ \frac{1}{M_i} + \frac{1}{M_j} \right]^{\frac{1}{2}} \quad (\text{S8-3})$$

The  $D_K$  depends on temperature, molar mass of the diffusing species, and pore diameter, calculated according to (S8-4)<sup>10</sup>:

$$D_K = \frac{1}{3} d_p \sqrt{\frac{8RT}{\pi M_i}} \quad (\text{S8-4})$$

## NOMENCLATURE

$a_s$  = external catalyst specific surface area ( $\text{m}^2 \text{g}^{-1}$ )

$C_a$  = Carberry number

$C_i^*$  = concentration of the reactant in bulk phase ( $\text{mol m}^{-3}$ )

$C_i$  = concentration inside of the NAHS ( $\text{mol m}^{-3}$ )

$C_o$  = concentration outside of the NAHS ( $\text{mol m}^{-3}$ )

$d$  = diameter of hollow sphere (m)

$dC_i/dx$  = concentration gradient of reactant ( $\text{mol m}^{-3} \text{m}^{-1}$ )

$D_B$  = bulk diffusion coefficient ( $\text{m}^2 \text{s}^{-1}$ )

$D_{eff}$  = effective diffusion coefficient ( $\text{m}^2 \text{s}^{-1}$ )

$D_{ij}$  = the diffusion coefficients for a binary mixture of i and j ( $\text{m}^2 \text{s}^{-1}$ )

$D_K$  = Knudsen diffusion coefficient ( $\text{m}^2 \text{s}^{-1}$ )

$D_p$  = diffusion coefficient ( $\text{m}^2 \text{s}^{-1}$ )

$J_D$  = Colburn J factor

$k_g$  = solid-gas mass transfer coefficient ( $\text{m}^3 \text{m}^{-2} \text{s}^{-1}$ )

$l$  = length of nanotube on NAHS (m)

$m$  = weight of catalyst (g)

$N$  = total quantity of hollow spheres per gram catalyst ( $\text{g}^{-1}$ )

$N_D$  = diffusion flux ( $\text{mol m}^{-2} \text{s}^{-1}$ )

$Q_c$  = chemisorption of hydrogen ( $\text{mol} \cdot \text{g}_{\text{cat}}^{-1}$ )

$Q_p$  = physisorption of hydrogen ( $\text{mol} \cdot \text{g}_{\text{cat}}^{-1}$ )

$Q_t$  = total amount of absorbed hydrogen ( $\text{mol} \cdot \text{g}_{\text{cat}}^{-1}$ )

$r_{\text{obs}}$  = observed reaction rate ( $\text{mol s}^{-1} \text{g}_{\text{cat}}^{-1}$ )

$R$  = radius of the catalyst particle (m)

$Re$  = Reynolds number

$S$  = surface area of a single NAHS ( $\text{m}^2$ )

$Sc$  = Schmidt number

$V_s$  = volume of a single hollow sphere ( $\text{m}^3$ )

$V_t$  = total volume of hollow sphere in per gram NAHS ( $\text{m}^3 \cdot \text{g}_{\text{cat}}^{-1}$ )

$V_i$  = atomic diffusion volumes ( $\text{m}^3$ )

$y_i$  = mole fraction of i

$\alpha$  = the weight of hollow sphere surface per unit area ( $\text{g} \cdot \text{m}^{-2}$ )

$\beta$  = remaining amount of DMO after passing through the nanotubes on per unit area hollow sphere surface ( $\mu\text{mol} \cdot \text{m}^{-2}$ )

$\varepsilon$  = porosity of the catalyst

$\tau$  = tortuosity factor

$\eta\varphi^2$  = Wheeler-Weisz criterion

## REFERENCES

1. Werner, S.; Arthur, F. Controlled Growth of Monodisperse Silica Spheres in the Micron Size Range *J. Colloid. Inter. Sci.* **1967**, *26*, 7.
2. Hohenberg, P. Inhomogeneous Electron Gas. *Phys. Rev.* **1964**, *136*, B864-B871.
3. Perdew, J. Generalized Gradient Approximation Made Simple. *Phys. Rev. Lett.* **1996**, *77*, 3865-3868.
4. Carberry, J. In *Physico-Chemical Aspects of Mass Transfer in Heterogeneous Catalysis*.; SpringerVerlag: Berlin, 1987.
5. Ronchin, L.; Toniolo, L. Selective Hydrogenation of Benzene to Cyclohexene Catalyzed by Ru Supported Catalysts - Influence of the Alkali Promoters on Kinetics, Selectivity and Yield. *Catal. Today* **2001**, *66*, 363-369.
6. Zhao, Y.; Zhou, J.; Zhang, J.; Li, D.; Wang, S. Selective Hydrogenation of Benzene to Cyclohexene on a Ru/Al<sub>2</sub>O<sub>3</sub>/cordierite Monolithic Catalyst: Effect of Mass Transfer on the Catalytic Performance. *Ind. Eng. Chem. Res.* **2008**, *47*, 4641-4647.
7. Marziano, N.; Ronchin, L.; Tortato, C.; Vavasori, A.; Badetti, C. Catalyzed Beckmann Rearrangement of Cyclohexanone Oxime in Heterogeneous Liquid/solid System Part 1: Batch and Continuous Operation with Supported Acid Catalysts. *J. Mol. Catal. A* **2007**, *277*, 221-232.
8. Venkatesan, R.; Fogler, H. Comments on Analogies for Correlated Heat and Mass Transfer in Turbulent Flow. *AIChE J.* **2004**, *50*, 1623-1626.
9. Yue, H.; Zhao, Y.; Zhao, L.; Lv, J.; Wang, S.; Gong, J.; Ma, X. Hydrogenation of Dimethyl Oxalate to Ethylene Glycol on a Cu/SiO<sub>2</sub>/Cordierite Monolithic Catalyst: Enhanced Internal Mass Transfer and Stability. *AIChE J.* **2012**, *58*, 2798-2809.
10. Poling, B, Prausnitz, J, Connell, J. In *The Properties of Gases and Liquids*.; New York: 2001.
11. Hill, J. In *An Introduction to Chemical Engineering Kinetics and Reactor Design*.; Wiley: New York, 1977.
12. Ramachadran, P. In *Three-Phase Catalytic Reactors*.; Gordon & Breach Science Publishers: New York, 1982.
13. Robert, G. In *Catalysis in Organic Synthesis*.; Academic Press: New York, 1976.